Title	An experimental study of menopause induced by bilateral ovariectomy and mechanistic effects of mesenchymal stromal cell therapy on the parotid gland of a rat model
Author(s)	El-naseery, Nesma Ibraheim; Elewa, Yaser Hosny Ali; Ichii, Osamu; Kon, Yasuhiro
Citation	Annals of anatomy - Anatomischer anzeiger, 220, 9-20 https://doi.org/10.1016/j.aanat.2018.06.006
Issue Date	2018-11
Doc URL	http://hdl.handle.net/2115/76001
Rights	© 2018. This manuscript version is made available under the CC-BY-NC-ND 4.0 license http://creativecommons.org/licenses/by-nc-nd/4.0/
Rights(URL)	http://creativecommons.org/licenses/by-nc-nd/4.0/
Type	article (author version)
File Information	AANAT2786R2.pdf

An experimental study of menopause induced by bilateral ovariectomy and mechanistic effects of mesenchymal stromal cell therapy on the parotid gland of a rat model

Nesma Ibraheim El-naseery†[1], Yaser Hosny Ali Elewa†[1,2]*, Osamu Ichii[2], Yasuhiro Kon[2]

[1]

Department of Histology and Cytology, Faculty of Veterinary Medicine, Zagazig University, Zagazig 44519, Egypt

[2]

Laboratory of Anatomy, Basic Veterinary Sciences, Faculty of Veterinary Medicine, Hokkaido University, Sapporo 060-0818, Japan

† Both authors contributed equally to this manuscript

*Corresponding author: Yaser Elewa, DVM, PhD,

- Laboratory of Anatomy, Basic Veterinary Sciences, Faculty of Veterinary Medicine, Hokkaido University, Kita 18, Nishi 9, Kita-ku, Sapporo 060-0818, Japan

- Department of Histology and Cytology, Faculty of Veterinary Medicine, Zagazig University, Zagazig 44519, Egypt

Tel: 008011-706-5188   Fax: 008011-706-5189

Email: y-elewa@vetmed.hokudai.ac.jp, yaserelewa@zu.edu.eg

Abstract:

The current study was conducted on a menopause rat model induced by ovariectomy to assess the histological and immunohistochemical alterations in the parotid glands and to verify the efficiency of human umbilical cord derived-mesenchymal stromal cell (hUCB-MSCs) in treating this condition. Eighteen adult female rats were equally divided into three groups: sham-operated (SHAM), ovariectomized (OVX) and OVX injected with hUCB-MSCs (OVX + hUCB-MSCs). At 3 months post-ovariectomy, the salivary flow rate and size of the parotid glands were measured. The parotid glands were histologically investigated via H&E stained sections. Furthermore, immunohistochemical analysis for human CD105, human CD34, proliferating cell nuclear antigen (PCNA), single strand DNA (ssDNA), Caspase 3, aquaporin (AQP)1, α-Smooth Muscle Actin (α-SMA) and mouse CD34 were performed. The OVX group showed interstitial hemorrhage, dispersed acini and intracytoplasmic vacuoles in the acinar cells. Furthermore, immunohistochemical staining revealed a significant decrement in the number of ssDNA positive apoptotic cells, but a significant increment of PCNA positive proliferating cells, AQP1 positive blood capillaries, α-SMA positive myoepithelial cells and endogenous CD34 positive hematopoietic progenitor cells in the OVX + hUCB-MSCs group as compared with the OVX group. These findings suggest a potential regenerative therapy of MSCs to injured parotid gland structures. However, further investigations are required to illustrate the mechanism of hUCB-MSCs mediated parotid gland regeneration.

1 **Abbreviations:**

2 α-SMA: Alpha-Smooth Muscle Actin

3 AQP1: Aquaporin1

4 Er: Estrogen receptor

5 hUCB: human Umbilical Cord Blood

6 hUCB-MCs: human Umbilical Cord Blood-Derived Mesenchymal Stromal Cells

7 MSCs: Mesenchymal Stromal Cells

8 OVX: Ovariectomized

9 PCNA: Proliferating Cell Nuclear Antigen

10 SHAM: Sham-operated

11 ssDNA: Single Stranded DNA

12

13

14

15

16

1. Introduction

In mammals, the saliva plays several essential roles including the protection of the oral cavity apparatus and the gastrointestinal epithelium. Moreover, it facilitates tasting, mastication, swallowing, and even digestion of food (Logemann et al., 2001). The parotid gland is one of the major salivary glands. Upon stimulation, it secretes over 50% of the total body saliva (Humphrey and Williamson, 2001). Salivary gland hypofunction is frequently observed in mammals and manifested by xerostomia (dry mouth) that leads to functional oral disorders. Xerostomia is associated with aging and many other systemic diseases (Yeh et al., 1998), and is frequent among menopausal females (Frutos et al., 2002). Additionally, it is frequently observed after radiotherapy (Jeong et al., 2013) and as a side effect of certain medications (Mortazavi et al., 2014).

The menopause is not a unique phenomenon to only human females, but it also occurs in a number of animals with longer lives, including the primate species (Walker and Herndon, 2008). Experimentally, the animal model of menopause could be achieved via bilateral ovariectomy (Arafat et al., 2016). Decline of estrogen (E2) levels during menopause is considered to be a major change that leads to many changes in the body (Messina et al., 2013). Interestingly, Rahnama et al. (2004) reported a correlation between the dryness of the mouth and the E2 deficiency, and owed it to the presence of high-affinity E2 receptors (ER), especially ER-β, in the major salivary glands of rats. Additionally, Gejima et al. (2007) detected ER-α in the parotid gland of adult female rats. The severe affection of the parotid gland in menopausal animal models has also been documented (Kusunoki et al., 2006; Mohamed et al., 2015).

35   Apoptosis refers to programmed cell death that occurs in tissues to maintain homeostasis in the body.

36   Lewis-Wambi and Jordan (2009) noticed that E2 regulates proliferation and apoptosis of many cell types.

37   Recently, association between E2 deficiency and histological alterations induced by apoptosis in the rat's

38   parotid gland has been noticed (Kusunoki et al.,2004). This apoptotic induction is caused mainly by free

39   radicals (Kusunoki et al., 2006).

40   All therapeutic approaches to the treating of menopausal symptoms via hormonal replacement are associated

41   with the possibility of venous thrombotic complications (Bińkowska, 2014), breast cancer, and gynecological

42   cancers (Bregar et al., 2014). In addition, herbal therapy also has serious side effects including

43   gastrointestinal disorder and abnormal vaginal bleeding (Xu et al., 2012), which restrict its clinical

44   applications and encourage researchers to find safe and effective alternate therapies for the treatment of

45   menopausal symptoms.

46   In the past decade, tissue engineering, particularly stem/stromal cell regenerative medicine, has made

47   significant advances in terms of restoration of the normal tissue functions. Mesenchymal stromal cells

48   (MSCs) have been successfully isolated from bone marrow (BM) (Jiang et al.,2002), adipose tissue (Eirin et

49   al.,2012), peripheral blood (PB) (Wan et al.,2006), and human umbilical cord blood (hUCB) (Hill et

50   al.,2009). The unique feature of MSCs is the immunological property of positivity for CD105, CD73, and

51   CD90 while lacking the expression of CD34, CD19, CD45, and HLA-DR surface molecules (Dominici et al.,

52   2006). The hUCB-MSCs are considered as one of the most easily available, least immunogenic and legal

53   materials (Ding et al., 2015), having the high potential for expansion and plasticity (El Maadawi and Gabr,

54   2011). Moreover, Doi et al. (2016) proved their safety in *in vitro* culture. Surprisingly, both E2 and hMSCs

55   exhibit similar antioxidant capacity and trophic effects (Valle-Prieto and Conget, 2010). In addition, Zhang

56   et al., (2012); Li et al. (2015) reported that, in high glucose culture, MSCs can differentiate into

57   steroidogenic cells which synthesize and secrete E2.

58   Interestingly, stromal cells have been successfully used to treat many diseases such as diabetes mellitus

59   (Soria et al., 2001), brain injury (Bang et al., 2005), cardiovascular diseases (Kawada et al., 2004; Dosi et al.,

60   2014), and several disorders associated with ovariectomy such as myocardial ischemia (Ray et al., 2008),

61   urinary incontinence (Lin et al., 2010), osteoporosis (Huang et al., 2016), and cerebellar disorders (Ahmed et

62   al., 2017). Despite the severe affection of the parotid gland in menopausal animal models and side effects of

63   its hormonal or herbal therapy, a new approach for its treatment is lacking. Therefore, the purpose of this

64   study was to evaluate histological and immunohistochemical structural alterations in the parotid gland of a

65   menopausal model, induced by abrupt E2 deficiency via ovariectomy in adult female albino rats and the

66   potential therapeutic roles of hUCB-MSCs.

67

68

69

70

71

72

2. Material and methods

2.1. Isolation and preparation of MSCs from hUCB

This isolation of cells was done in the clinical chemistry and stem cell lab, in the Medical Biochemistry &

Molecular Biology Department, Faculty of Medicine, at Zagazig University, Egypt.

Collection of hUCB sample

Cord blood was obtained under complete aseptic conditions from the umbilical vein of six post-delivery

full-term placentae at Zagazig University Hospital after getting informed consent from husbands and

approved by the Institutional Review Board (IRB), Zagazig University (ZU-IRB #4626). The

samples were directly collected in a sterile 50 mL Falcon tubes containing 2 mL ethylene diamine tetraacetic

acid (EDTA) (Lonza Bioproducts, Belgium) and 5 mL of phosphate buffer saline (PBS) of pH 7.2. Then, the

samples were transported (maintaining temperature between 15-22°C) to the clinical chemistry and stem cell

lab for isolation of stromal cells.

2.1.1. Isolation and Culture of hUCB derived MSCs

The collected blood was diluted three times with PBS. Then, 30 ml of diluted blood was carefully loaded on

10 mL of Ficoll/Paque (Lymphocyte Separation Medium 1.077, Lonza Bioproducts, Basel, Switzerland) in

50 mL centrifuge tubes. The centrifugation was done at 435 g for 30 min at 22°C. After removal of the

supernatant and careful aspiration of the mononuclear cells' (MNCs) layer, the MNCs were washed with

PBS twice and centrifuged at 20°C for 10 min. Finally, the MNCs were isolated and the supernatant was

91 discarded. The isolated MNCs were subcultured in DMEM (Dulbecco's modified Eagles medium) (Cambrex

92 Bio Science, Minnesota, USA) supplemented with 10% fetal bovine serum (FBS, Lonza Bioproducts, Basel,

93 Switzerland) and 1% penicillin-streptomycin-amphotericin B mixture as 10 IU /25 mg/100 ml (Lonza

94 Bioproducts, Belgium) at a concentration of 5000 cm^{-2} $(0.2–0.3$ ml media$)^{-1}$. The culture was incubated at

95 37°C in 5% humidified CO2 in a CO2 incubator (Heraeus, Germany). After overnight incubation (12-18

96 hours), the media were replaced in order to eliminate non-adherent cells. The media were replaced every 3

97 days for 12–14 days until colonies of MSC were noticed as spindle-shaped fibroblastoid cells of the first

98 passage culture (at 80-90% confluence) under the inverted microscope. At 37°C for 5 min, colonies were

99 released with 0.25% trypsin in 1 ml EDTA. Immediately after trypsinization and centrifugation, subculturing

100 was done in serum-supplemented medium and incubated in 50 cm^2 tissue culture flask until adhesiveness and

101 fusiform shape of MSCs were obtained (Bieback et al., 2004). The fourth passage of culture was used after

102 labeling with fluorescent marker using Paul Karl Horan 26 (PKH-26) Fluorescent Cell Linker Kit

103 (Sigma-Aldrich Chemie, Steinheim, Germany) obtained from Algomhuria Co (Mohafza st., Zagazig, El

104 Sharqia, Egypt) as per the protocol described by Haas et al. (2000).

105   *2.1.2.   Immunophenotypic characterization of hUCB-MSCs by flow cytometry applications*

106 Based on stromal cell surface markers, we used monoclonal antibodies against human CD105 and CD90

107 (mesenchymal stromal cell surface marker) (20% cutoff) (Zheng et al.,2013). We also used monoclonal

108 antibodies against human CD34 and CD45 to exclude hematopoietic, endothelial cells, and leukocytes. All

109 the antibodies were obtained from BD Bioscience. The detached cells were washed twice with PBS and

110   incubated with either anti-human CD105 (Cat No: 323205), CD90 (Cat No: 559869), CD34 (Cat No:

111   4084644), or CD45 (Cat No: 349202) according to manufacturer's instructions, for 30 min in the dark. Cells

112   were analyzed by FACS Scan 3 color (Becton Dickinson, Heidelberg, Germany) running Cell Quest

113   software (BD, San Joe, USA), in the Clinical Pathology laboratories, Zagazig University.

114   **2.2. Animals and experimental ethics**

115   Eighteen female albino rats (6-months old) were obtained from the animal house, Faculty of Veterinary

116   Medicine, Zagazig University, Egypt. The rats were housed in individual stainless-steel cages in a clean

117   room with controlled temperature (23°C) and humidity (60%), and with a 12 h dark/light cycle. The animals

118   were given a standard diet and tap water ad-libitum. The authors adhered to the Guide for the Care and

119   Use of Laboratory Animals of Zagazig University. The experimental protocols described in this research

120   were approved by the Institutional Review Board (IRB), Zagazig University (ZU-IRB #4626). The rats were

121   divided equally into three groups (n=6): sham-operated (SHAM), ovariectomized (OVX), and OVX +

122   hUCB-MSCs. The OVX + hUCB-MSCs group received an injection of 4.5 x 10^6 hUCB-MSCs dissolved in

123   250 μL PBS on the tail vein two months after ovariectomy for four consecutive weeks (twice in a week)

124   (Calatrava-Ferreras et al., 2012). However, both SHAM and OVX groups were injected with vehicle (PBS)

125   only.

126   **2.3. Ovariectomy procedure**

127   The ovariectomy was performed by method described by Huang et al. (2016) under complete aseptic

128   conditions ten days after acclimatization of rats. Briefly, all rats were anesthetized by intraperitoneal

129 injection of 1% Na pentobarbital. After the onset of anesthesia, clipping and shaving the skin was done, then

130 aseptic scrubbing with alcohol and povidone iodine. A short dorsal midline skin incision was made halfway

131 between the caudal edge of the rib cage and the base of the tail bilaterally with a surgical blade (No. 11).

132 Opening the muscles and peritoneal cavity, the adipose tissue was retracted until the ovaries were identified

133 which were then excised after ligation of their blood supply using 3-0 vicryl. At the end of the surgical

134 procedures, the peritoneum and abdominal muscles were closed using 3-0 vicryl and the skin suture was

135 done with 2-0 nylon. After the surgery, rats were allowed to live in normal environment. They were given

136 ampicillin (4000 IU/kg, intraperitoneal) for 3 days. The rats were subcutaneously given non-steroidal

137 anti-inflammatory drug meloxicam (0.2 mg/kg) once daily for 3 successive days. The wound dressing was

138 applied every day for a week to prevent the risk of infection. For SHAM group, both ovaries were exposed

139 and only mobilized.

140 **2.4. Salivary flow rate**

141 Under the effect of anesthesia (intramuscular injection of a mixture of ketamine Hcl (50 mg/kg) and xylazine

142 Hcl (5 mg/kg)), saliva was collected from all rats two to three minutes after pilocarpine was injected

143 subcutaneously. Saliva was flowed freely into a sterile glass pipettes for a period of 30 min for each rat and

144 was then harvested. Salivary flow rate was presented as microliters per minute.

145 **2.5. Tissue preparation for microscopic observation**

146 At 3 months post-ovariectomy, rats from all experimental groups were euthanized under inhalational

147 anesthesia. The parotid glands were dissected, weighed, and immediately fixed in 4% paraformaldehyde

148   solution. After overnight fixation, parotid gland specimens were dehydrated in graded alcohol and embedded

149   in paraffin. Then, 3-μm thick paraffin sections were deparaffinized, rehydrated, stained with hematoxylin

150   and eosin (H&E), and observed under light microscope, and photographed with the Amscope digital camera

151   (Bancroft and Layton, 2013).

152   For the detection of the PKH26-labelled hUCB-MSCs homing, 3-μm thick deparaffinized sections of all

153   groups were examined and photographed with a fluorescence microscope (Olympus BX50F4, No. 7M03285,

154   Tokyo, Japan).

155   **2.6. Immunohistochemistry**

156   The immunohistochemical analyses for human CD105 and human CD34, proliferating cell nuclear antigen

157   (PCNA), caspase 3 and single strand DNA (ssDNA), aquaporin (AQP)1, α smooth muscle actin (SMA), and

158   mouse-CD34 were performed to detect hUCB-MSCs homing, proliferating cells, apoptotic cells, blood

159   capillaries, myoepithelial cells, and endogenous hematopoietic progenitor cells, respectively (Elewa et al.,

160   2010). In brief, antigen retrieval was done with the deparaffinized sections according to each antibody (Table

161   1). Then sections were incubated in methanol containing 0.3% H_2O_2 for 20 minutes at 4°C to block the

162   activity of endogenous peroxidase, followed by washing in distilled water, and incubation with 10% normal

163   blocking serum for 1 h at room temperature (donkey serum for PCNA immunostaining and goat serum for

164   staining of the other antigens). Then sections were incubated overnight with the specific primary antibody

165   diluted in PBS (pH 7.2). The antibodies and working dilutions are shown in Table 1. For negative control,

166   the primary antibody was replaced with only PBS. Then the sections were incubated with biotin-conjugated

167   secondary antibody, specific to the primary one, for 30 min, followed by incubation for 30 min with

168   streptavidin-peroxidase conjugate. The positive reaction was visualized with 3, 3′-diaminobenzidine

169   tetrahydrochloride (DAB)-H2O2 solution, pH 7.0. Finally, the sections were washed in distilled water and

170   counterstained with Mayer's hematoxylin.

171   **2.7. Histoplanimetrical analysis**

172   The number of immunopositive PCNA, ssDNA, caspase 3, and mouse-CD34 cells were counted in

173   immunohistochemical stained sections at 400 x magnification. In addition, the integrated density of AQP1 and

174   α-SMA were evaluated using Photoshop (Adobe Systems, San Jose, Calif., USA) followed by Image J analysis

175   software (ver. 1.32j, http://rsb.info.nih.gov/ij). Briefly, using Photoshop we converted the RGB color images

176   into grayscale to reduce the background color. Then, using threshold, we highlighted the signal into black color

177   with a white background and inverted the signal color from black to white and saved the images. Subsequently,

178   we analyzed the integrated density of the white signals on the processed images using Image J software.

179   **2.8. Statistical analysis**

180   All statistical analysis results were expressed as mean ± standard error (SE). The one-way ANOVA test was

181   used to analyze the data among different groups, followed by multiple comparisons Duncan′s Post-hoc test

182   when significant differences were observed ($P < 0.05$) (n=6 per group).

183

184

185

186

187   **3.   Results**

188   **3.1. Characterization of hUCB-MSCs and homing of PKH26-labeled hUCB-MSCs in parotid gland**

189   Morphologically, MSCs culture at day 7 of isolation showed fusiform-shaped cells (Fig. 1A). The flow

190   cytometric analysis of the hUCB-MSCs culture revealed that the cells had a positive expression for human

191   CD105 (85.65%) and human CD90 (62.33%), while a negative expression for human CD34 (1.36%) and

192   human CD45 (2.19%) were detected (Fig. 1B). To confirm the homing of PKH26-labeled hUCB-MSCs,

193   3-μm thick deparaffinized sections of all groups were examined. The MSCs were detected in the parotid

194   gland sections of the OVX + hUCB-MSCs group (3 months post-ovariectomy) as red fluorescence between

195   acini and ducts (Figs. 2A and B) but not in other groups (data not shown). Furthermore, a positive reaction

196   for human CD105 was observed around the acini and ducts (Fig. 2C), while the human CD34 expression was

197   not detected (Fig. 2D).

198   **3.2. Salivary flow rate and weight of parotid glands**

199   As shown in Table 2, both the salivary flow rate and the weight of parotid glands were significantly

200   decreased in the OVX group when compared to the SHAM group. After hUCB-MSCs injection, a significant

201   increase was observed by comparison with that of the OVX group.

202   **3.3. Histological observations**

203   Examination of H&E stained sections revealed that the parotid gland of SHAM group was a

204   multilobulated organ. Each lobule was formed of a closely packed serous acini and a series of duct

205   systems. All serous acini had very narrow lumina that could hardly be seen and were lined with

206   pyramidal acinar cells. The acinar cell cytoplasm exhibited apical acidophilia and basal basophilia

207   with basal rounded nuclei containing prominent nucleoli. The intralobular duct system was

208   composed of intercalated ducts and striated ducts. Both ducts were lined with cuboidal and

209   columnar epithelial cells, respectively, with acidophilic stained cytoplasm. The striated ducts were

210   the predominant ducts (Fig. 3A). In the OVX group, the acini were dispersed with lightly stained

211   cytoplasm. The acinar cells lining the acini had numerous cytoplasmic vacuoles and some

212   crescent-shaped nuclei. The striated duct had darkly stained nuclei and an ill-defined basal

213   striation. Additionally, an interstitial hemorrhage was pronounced (Fig. 3B). An observable

214   improvement of the parotid gland architecture was noticed in the OVX + hUCB-MSCs group with

215   apparently normal structures of both acinar cells and striated ducts (Fig. 3C).

216   **3.4. Immunohistochemical observations**

217   The immunohistochemical staining with anti-PCNA was performed to detect proliferating cells. The positive

218   cells were observed in the acini of the three different experimental groups, as expected (Figs. 4A, B, and C),

219   while the negative control immunostained sections of the parotid gland of the SHAM group revealed absence

220   of any positive reaction (Fig. 4D). The expressions of positive cells were significantly decreased in the OVX

221   group (10.56± 0.63), compared to the SHAM group (30.08± 2.51), while they were considerably higher in

222   the OVX + hUCB-MSCs group (23.28± 1.42) compared to the OVX group (Fig. 4E).

223 Immunohistochemical staining for caspase 3 and ssDNA were performed to observe apoptotic cell

224 populations. The caspase 3 positive apoptotic cells were observed in the interstitial cells of the three groups

225 (Figs. 5A, B, and C). The negative control sections of the parotid gland of the OVX group revealed the

226 absence of apoptotic cells (Fig. 5D). In the OVX group, there was a significant increase in caspase 3

227 apoptotic cells (11.17 ± 0.76), compared to the SHAM group (0.83 ± 0.17), while the frequency of such

228 apoptotic cells was significantly decreased in the OVX + hUCB-MSCs group (3.11 ± 0.44) compared to the

229 OVX group (Fig. 5E). The other apoptotic cell marker was ssDNA that were mainly detected in both acinar

230 and ductal epithelium (data not shown) of the OVX group, while they were hardly to be seen in the SHAM

231 and OVX + hUCB-MSCs groups. The OVX group showed a significant increase in ssDNA positive cells

232 (101 ± 14.18), compared to the SHAM group (1.22 ± 0.55). On the other hand, the number of ssDNA

233 positive cells was much less in the OVX + hUCB-MSCs group; however, a non-significant difference was

234 observed in the average number of the ssDNA positive cells in the OVX + hUCB-MSCs group (4.44 ± 1.3)

235 when compared with that of the SHAM group (Fig. 5F).

236 The immunohistochemical staining with anti-AQP1 was performed to examine the alterations of the blood

237 capillaries among the three different groups. The endothelial cells of blood capillaries showed positive

238 reactions for AQP1 in all groups (Figs. 6A, B, and C). No positive reaction was observed in the negative

239 control sections of the parotid gland in the SHAM group (Fig. 6D). The integrated density of AQP1 positive

240 reactions showed a significant reduction in the OVX group ($15.02 \times 10^6 \pm 1.35$), compared with the SHAM

241 group ($31.24 \times 10^6 \pm 3.77$). However, an increase in the integrated density of AQP1 positivity was observed

13

242   in the OVX + hUCB-MSCs group (29. 05 X 10^6 ± 2.87), compared to the OVX group. However, there was

243   no significant difference in the integrated density of AQP1 positivity was observed in the OVX +

244   hUCB-MSCs group compared to that observed in the SHAM group (Fig. 6E).

245   The changes in myoepithelial cell populations were investigated in different experimental groups via

246   immunohistochemical staining with anti-α-SMA. Interestingly, the myoepithelial cell populations showed a

247   great variation among different groups. Well-developed α-SMA positive myoepithelial cells with numerous

248   cytoplasmic processes were observed around the acini of the parotid glands of the SHAM group (Fig. 7A),

249   while the myoepithelial cells after ovariectomy showed fewer and shorter processes (Fig. 7B). In the OVX +

250   hUCB-MSCs group, the cytoplasmic processes showed moderate development (Fig. 7C). The negative

251   control sections of the parotid gland of the SHAM group showed no positive reaction (Fig. 7D). These

252   findings were confirmed by analyzing the integrated density of immunopositive cytoplasmic processes. The

253   integrated density of positive reactions showed a significant decrement in the OVX group (33.99 X 10^6 ±

254   4.48) when compared to the SHAM group (141.22 X 10^6 ± 11.55). However, following treatment with

255   hUCB-MSCs, a higher integrated density of positive reactions was observed in the OVX + hUCB-MSCs

256   group (95.85 X 10^6 ± 5.82) compared to that of the OVX group (Fig. 7E).

257   Immunohistochemical staining using mouse CD34 antibody in the parotid gland sections of different

258   experimental groups was performed to evaluate the endogenous hematopoietic progenitor cell populations

259   (Figs. 8A, B, and C). The negative control sections of the parotid gland of the SHAM group revealed no

260   positive reactivity (Fig. 8D). A significant loss of CD34 positive cells was observed in the OVX group (0.33

261   ± 0.21) as compared with the SHAM group (12.33 ± 1.28), but their expression was markedly restored in the

262   OVX + hUCB-MSCs group (12.17 ± 1.35) in which there was no significant difference compared to the

263   SHAM group (Fig. 8E).

264

265

266

267

268

269

270

271

272

273

274

275

276

277

4. Discussion

During the female reproductive cycle, E2 promotes salivary glands growth and mediates changes in saliva's

chemical composition (Valimaa et al.,2004) owing to the presence of ER-β (Rahnama et al.,2004) and ER-α

(Gejima et al.,2007) in the parotid gland of adult female rats. Therefore, in the present study, we investigated

the influence of abrupt E2 deficiency on the parotid gland structure via ovariectomy of adult female albino

rats. Moreover, we examined the potential therapeutic roles of hUCB-MSCs on the parotid gland architecture

following ovariectomy.

Both parotid glands weight and salivary flow rate were significantly decreased in the OVX group in

comparison to the SHAM group, as previously reported (Abd El-Haleem et al.,2018). It was confirmed in the

present study by our observations of the glandular architecture that showed numerous intracytoplasmic

vacuoles in the acinar cells of rats of OVX group. Similar atrophic changes in the parotid glands were

reported in radiated rats (Jeong et al., 2013) and in rats after bilateral ovariectomy (Parlak et al., 2014, Abd

El-Haleem et al., 2018). The cellular vacuolization is considered by Myers and McGavin (2007) as an early

sign of cellular degeneration. Deficiency of the trophic effects of E2 (Valimaa et al., 2004) and increment in

apoptosis (Kusunoki et al. 2006) may be the causes of these structural alterations. In the present study,

ovariectomy caused a statistically significant decrement of proliferative cell populations and increment of

apoptotic cells as compared to the SHAM group. The apoptotic cells expressed positive caspase 3 in the

interstitial tissues and ssDNA in both acinar and ductal cells of the OVX group. On the other hand, Limesand

296 et al. (2006) found caspase 3 activation in the acinar cells of both parotid and submandibular glands of

297 gamma-irradiated mice. The caspase-3 is required for DNA fragmentation and some of the typical

298 morphological alterations in cells during apoptosis (Jänicke et al., 1998). Therefore, the apoptotic cells were

299 identified based on early events (activation of caspase-3, keratin 18 cleavage) or late events (nuclear

300 condensation, DNA fragmentation) in the apoptosis pathway as reported by Krysko et al. (2008). We

301 proposed that the interstitial apoptotic cells could be myoepithelial cells. Both apoptotic and proliferating

302 myoepithelial cells were detected in the submandibular glands of atrophic rats via duct ligation (Takahashi et

303 al., 2001). The results of the present study were reinforced by the observations of Limesand et al. (2006),

304 who clarified that glandular homeostasis requires a balance in cell proliferation and apoptosis.

305　　　　Interestingly, the ovarectomized rats showed impairment of acinar and ductal structures with

306 reduction of myoepithelial cell processes, which might explain xerostomia in the menopausal human or

307 long-lived animals.

308 Recently, therapeutic approaches via stromal cells have successfully been used in many disorders such as

309 radiation-damaged rat salivary glands (Jeong et al.,2013) and damage of parotid glands in ovariectomized

310 rats via bone marrow-MSCs (Abd El-Haleem et al.,2018). In the current work, we chose hUCB-MSCs to

311 treat the OVX-induced damage of parotid glands due to their unique biological characteristics. The

312 hUCB-MSCs are more advantageous than bone marrow-MSCs in this context since they are younger and

313 have a wider differentiation capability (Zhao et al., 2016).

17

314   After hUCB-MSCs injection in this study, we observed apparently normal acinar cells and striated ducts in

315   H&E stained sections. In addition, the increased proliferative cells and decreased apoptotic cells in the

316   immunostained sections may suggest that MSCs may act through paracrine mechanisms via anti-apoptotic

317   factors including cytokines (Takahashi et al.,2006), stanniocalcin-1, and vascular endothelial growth factor

318   (Doorn et al., 2012) to mediate tissue repair and regeneration.

319   The AQP1 is a water channel found in the endothelial cell of blood capillaries. These channels play an

320   important role in water permeability (Li et al., 1994). Therefore, decrement of AQP1 expression in our OVX

321   group denoted dysfunction of the blood capillaries that coincided with the noticeable interstitial hemorrhage.

322   These findings are in support of the previous report of Jin et al. (2012) who demonstrated that AQP1 was

323   influenced by E2 deficiency. Smith et al. (2009) added that E2 and progesterone deficiency influence the

324   balance between vasoconstriction and vasodilatation in the submandibular gland. In our study, the

325   improvement of AQP1 densities in the OVX + hUCB-MSCs group may be due to the neovascularization

326   (Takahashi et al., 2006; Lim et al., 2013) via angiogenic cytokines (Takahashi et al., 2006) and endothelial

327   cell-derived clusterin molecules (Mishima et al., 2012) secreted by h-MSCs. Jin et al. (2012) confirmed that

328   the AQP1 play an important role in regulating body electrolyte balance and fluid secretion. In 2016, Teos et

329   al. and Delporte et al. demonstrated that AQP1 has a definite role in saliva secretion that was proved via

330   increase in saliva secretion after an intraductal injection of human AQP1 incorporated with adenovirus.

331   Our study used integrated density of α SMA-positive area on immunostained sections as an index of the

332   changes in myoepithelial cell populations. These densities were significantly decreased in the OVX group

333   whereas they significantly increased after hUCB-MSCs treatment. This obvious myoepithelial loss clarifies

334   its role in glandular hypofunction associated with ovariectomy, as previously reported by Safayi et al.

335   (2012).

336   The most interesting finding is the presence of endogenous $CD34^+$ hematopoietic progenitor cells around

337   acini and ducts in the parotid glands of SHAM group. $CD34^+$ is a cell surface marker of hematopoietic

338   stem/stromal cells and hematopoietic progenitor cells (Sidney et al., 2014). These cells are identified as side

339   population (SP) cells (Mishima et al., 2012). Our findings revealed the ovariectomy-induced depletion of

340   endogenous $CD34^+$ hematopoietic progenitor cells via apoptosis. Such findings are similar to that produced

341   by irradiation that leads to the damage of self-renewal property of hematopoietic stromal cell in mononuclear

342   cells isolated from bone marrow of mice (Wang et al., 2006). In our study, the mechanism of $CD34^+$

343   hematopoietic progenitor cells recovery may be via angiocrine (Kobayashi et al., 2010) and pleiotrophin

344   (Himburg et al., 2010) growth factors that were secreted from recovered endothelial cells. Sidney et al.

345   (2014) reported that the regenerative functions of endogenous stromal cells occur by providing molecular

346   signals to the proliferating immature epithelial cells in the forms of basement membrane proteins,

347   extracellular matrix, matrix metalloproteinases/proteases, and growth factors. Further investigations are

348   required for further elucidation of the mechanism of hUCB-MSCs mediated parotid gland regeneration.

349   In summary, our results suggest that the bilateral ovariectomy could affect the parotid gland structure due to

350   destruction of endothelial cells, and apoptosis of acinar and ductal cells. Interestingly, we revealed that most

351   of the structural injuries of the parotid gland were improved by hUCB-MSCs therapy. Such improvement in

352 mechanisms by MSCs might be via endothelial cells recovery and endogenous $CD34^+$ hematopoietic

353 progenitor cells rescue. Apoptosis inhibition and proliferation enhancement mechanisms of acinar and ductal

354 cells with myoepithelial cells recovery could also be responsible. Therefore, hUCB-MSCs therapy might be

355 a good alternative to treat parotid gland destruction, especially in menopausal cases, to evade the health risks

356 of hormonal therapy.

357 **FUNDING**

361

362

363

364

365

366

367

368

369

370

371

References

Abd El-Haleem, M.R., Selim, A.O., Attia, G.M., 2018. Bone marrow-derived mesenchymal stem cells ameliorate parotid injury in ovariectomized rats. Cytotherapy. 20(2), 204-217.

Ahmed, S.M., Abdelrahman, S.A., Shalaby, S.M., 2017. Therapeutic Potential of Mesenchymal Stem Cells vs. Estradiol Benzoate or Avosoya on the Cerebellar Cortex of Ovariectomized Adult Albino Rats. J. Cytol. Histol.8(1),1000444.

Arafat, E.A., Ghoneim, F.M., Khalaf, H.A., Elsamanoudy, A.Z., 2016. Anti-senescence role of coenzyme Q10 and 17 β-estradiol on submandibular gland of ovariectomized rats: histological, immunohistological and molecular studies. Int. J. Clin. Exp. Pathol. 9(11),10853-10870.

Bancroft, J., Layton, C., 2013. Hematoxylin and eosin. In: Suvarna SK, Layton C, Bancroft JD (eds) Theory and Practice of histological techniques, Ch. 10 and 11, Seventh Edition. Churchill Livingstone of Elsevier, Philadelphia, pp.172–214.

Bang, O.Y., Lee, J.S., Lee, P.H., Lee, G., 2005. Autologous mesenchymal stem cell transplantation in stroke patients. Ann. Neurol. 57(6), 874-882.

386   Bieback, K., Kern, S., Klüter, H., Eichler, H., 2004. Critical parameters for the isolation of mesenchymal

387   stem cells from umbilical cord blood. Stem Cells. 22, 625–634.

388   Bińkowska, M., 2014. Menopausal hormone therapy and venous thromboembolism. Prz Menopauzalny.

389   13(5), 267-272.

390   Bregar, A., Taylor, K., Stuckey, A., 2014. Hormone therapy in survivors of gynecological and breast

391   cancer. The Obstetrician & Gynaecologist. 16, 251–258.

392   Calatrava-Ferreras, L., Gonzalo-Gobernado, R., Herranz, A.S., Reimers, D., Montero Vega, T., Herranz,

393   A.S., Reimers, D., Vega, T.M., Jiménez-Escrig, A., López L.A.R., Bazán, E., 2012. Effects of

394   Intravenous Administration of Human Umbilical Cord Blood Stem Cells in 3-Acetylpyridine-Lesioned

395   Rats. Stem Cells Int. 2012, 135187.

396   Delporte, C., Bryla, A., Perret, J., 2016. Aquaporins in Salivary Glands: From Basic Research to

397   Clinical Applications. Int. J. Mol. Sci. 17(2),166.

398   Ding, D.C., Chang, Y.H., Shyu, W.C., Lin, S.Z., 2015. Human umbilical cord mesenchymal stem cells: a

399   new era for stem cell therapy. Cell Transplant. 24(3), 339-347.

400   Doi, H., Kitajima, Y., Luo, L., Yan, C., Tateishi, S., Ono, Y., Urata, Y., Goto, S., Mori, R., Masuzaki, H.,

401   Shimokawa, I., Hirano, A., Li, T.S., 2016. Potency of umbilical cord blood-and Wharton's jelly-derived

402   mesenchymal stem cells for scarless wound healing. Sci. Rep. 6, 18844.

403   Dominici, M., Le Blanc, K., Mueller, I., Slaper-Cortenbach, I., Marini, F., Krause, D., Deans, R.,

404   Keating, A., Prockop, D.J., Horwitz, E., 2006. Minimal criteria for defining multipotent mesenchymal

405   stromal cells. The International Society for Cellular Therapy position statement. Cytotherapy. 8,

406   315-317.

407   Doorn, J., Moll, G., Le Blanc, K., van Blitterswijk, C., de Boer, J., 2012. Therapeutic applications of

408   mesenchymal stromal cells: paracrine effects and potential improvements. Tissue Eng Part B Rev.

409   18(2),101-115.

410   Dosi, R., Bhatt, N., Shah, P., Patell, R., 2014. Cardiovascular disease and menopause. J. Clin. Diagn. Res.

411   8(2), 62-64.

412   Eirin Zhu, X.Y., Krier, J.D., Tang, H., Jordan, K.L., Grande, J.P., Lerman, A., Textor, S.C., Lerman,

413   L.O., 2012. Adipose tissue-derived mesenchymal stem cells improve revascularization outcomes to

414   restore renal function in swine atherosclerotic renal artery stenosis. Stem Cells. 30(5), 1030–1041.

415   Elewa, Y.H., Bareedy, M.H., Abuel-Atta, A.A., Ichii, O., Otsuka, S., Kanazawa, T., Lee, S.H.,

416   Hashimoto, Y., Kon, Y.,2010. Cytoarchitectural differences of myoepithelial cells among goat

417   major salivary glands. Vet. Res. Commun. 34, 557–567.

418   El Maadawi, Z.M., Gabr, H.M., 2011. Effect of human cord blood-derived stem cells on induced diabetic

419   retinopathy in adult albino rat: histological and immunohistochemical study. Egypt. J. Histol. 34,

420   576-585.

421   Frutos, R., Rodriguez, S., Miralles-Jorda, L., Machuca, G.,2002. Oral manifestations and dental

422   treatment in menopause. Med. Oral. 7(1), 26–30.

423   Gejima, K., Kawaguchi, H., Souda, M., Kawashima, H., Komokata, T., Hamada, N., Umekita, Y.,

424   Sakata, R., Yoshida, H., 2007. Expression of Estrogen Receptor-α Protein in the Rat Digestive Tract. in

425   vivo. 21(3), 487- 492.

426   Haas, S.J., Bauer, P., Rolfs, A., Wree, A., 2000. Immunocytochemical characterization of in vitro

427   PKH26-labelled and intracerebrally transplanted neonatal cells. Acta Histochem.102, 273-280.

428   Hill, A.J., Zwart, I., Tam, H.H., Chan, J., Navarrete, C., Jen, L.S., Navarrete, R., 2009. Human Umbilical

429   Cord Blood-Derived Mesenchymal Stem Cells Do Not Differentiate Into Neural Cell Types or Integrate

430   Into the Retina After Intravitreal Grafting in Neonatal Rats. Stem Cells and Develop. 18(3), 499-509.

431   Himburg, H.A., Muramoto, G.G., Daher, P., Meadows, S.K., Russell, J.L., Doan, P., Chi, J.T., Salter,

432   A.B., Lento, W.E., Reya, T., Chao, N.J., Chute, J.P., 2010. Pleiotrophin regulates the expansion and

433   regeneration of hematopoietic stem cells. Nat Med. 16(4), 475–482.

434   Huang, S., Xu, L., Sun, Y., Lin, S., Gu, W., Liu, Y., Zhang, J., Chen, L., Li, G., 2016. Systemic

435   Administration of Allogeneic Mesenchymal Stem Cells Does Not Halt Osteoporotic Bone Loss in

436   Ovariectomized Rats. PLoS ONE. 11(10), e0163131.

437   Humphrey, S.P., Williamson, R.T., 2001. A review of saliva: normal composition, flow, and

438   function. J. Prosthet. Dent. 85(2), 162-169.

439   Jänicke, R.U., Sprengart, M.L., Wati, M.R., Porter, A.G., 1998. Caspase-3 is required for DNA

440   fragmentation and morphological changes associated with apoptosis. J. Biol. Chem. 273, 9357–9360.

441   Jeong, J., Baek, H., Kim, Y-J., Choi, Y., Lee, H., Lee, E., Kim, E.S., Hah, J.H., Kwon, T.K., Choi, I.J.,

442   Kwon, H., 2013. Human salivary gland stem cells ameliorate hyposalivation of radiation-damaged rat

443   salivary glands. Exp. Mol. Med. 45, e58.

444   Jiang, Y., Jahagirdar, B.N., Reinhardt, R.L., Schwartz, R.E., Keene, C.D., Ortiz-Gonzalez, X.R., Reyes,

445   M., Lenvik, T., Lund, T., Blackstad, M., Du, J., Aldrich, S., Lisberg, A., Low, W.C., La rgaespada, D.A.,

446   Verfaillie, C.M., 2002. Pluripotency of mesenchymal stem cells derived from adult marrow. Nature. 418,

447   41-49.

448   Jin, P.Y., Lu, Y.C., Li, L., Han, Q.F., 2012. Coaction of CFTR and AQP1 increases permeability of

449   peritoneal epithelial cells on estrogen-induced ovarian hyperstimulation syndrome. BMC Cell Biol.13,

450   23.

451   Kawada, H., Fujita, J., Kinjo, K., Matsuzaki, Y., Tsuma, M., Miyatake, H., Muguruma, Y., Tsuboi, K.,

452   Itabashi, Y., Ikeda, Y., Ogawa, S., Okano, H., Hotta, T., Ando, K., Fukuda, K., 2004. Nonhematopoietic

453   mesenchymal stem cells can be mobilized and differentiate into cardiomyocytes after myocardial

454   infarction. Blood .104, 3581-3587.

455   Kobayashi, H., Butler, J.M., O'Donnell, R., Kobayashi, M., Ding, B.S., Bonner, B., Chiu, V.K., Nolan,

456   D.J., Shido, K., Benjamin, L., Rafii, S., 2010. Angiocrine factors from Akt-activated endothelial cells

457   balance self-renewal and differentiation of hematopoietic stem cells. Nat. Cell Biol. 12(11), 1046–1056.

458   Krysko, D.V., Berghe, T.V., D'Herde, K., Vandenabeele, P., 2008. Apoptosis and necrosis: Detection,

459   discrimination, and phagocytosis. Methods. 44, 205–521.

460   Kusunoki, T., Shiraishi, H., Murata, K., 2006. The role of estrogen and Cu, Zn-SOD on histological

461   changes after menopause in female rat parotid. Auris Nasus Larynx. 33(1), 47-51.

462   Kusunoki, T., Shiraishi, H., Murata, K., Nishida, N., Tomura, T., 2004. Apoptosis and estrogen on aging

463   changes of female rat parotids. Aging cell Acta Med. Kinki. Univ. 29, 27–30.

464   Lewis-Wambi, J.S., Jordan, V.C., 2009. Estrogen regulation of apoptosis: how can one hormone

465   stimulate and inhibit? Breast Cancer Res. 11(3), 206.

466   Li, J., Nielsen, S., Dai, Y., Lazowski, K.W., Christensen, E.I., Tabak, L.A., Baum, B. J., 1994.

467   Examination of rat salivary glands for the presence of the aquaporin CHIP. Pflugers. Arch. 428,

468   455–460.

469   Li, J., Peng, X., Zeng, X., Liu, B., Hao, Q., Yu, X., Zhu, L., Hu, Q., 2015. Estrogen Secreted by

470   Mesenchymal Stem Cells Necessarily Determines Their Feasibility of Therapeutical Application. Sci.

471   rep. 5, 15286.

472   Lim, J.Y., Ra, J.C., Shin, I.S., Jang, Y.H., An, H.Y., Choi, J.S., Kim, W.C., Kim, Y.M., 2013. Systemic

473   transplantation of human adipose tissue-derived mesenchymal stem cells for the regeneration of

474   irradiation-induced salivary gland damage. PloS One. 8(8), e71167.

475   Limesand, K.H., Schwertfeger, K.L., 2006. Anderson SM. MDM2 is required for suppression of

476   apoptosis by activated Akt1 in salivary acinar cells. Mol. Cell. Biol. 26, 8840-8856.

477   Lin, G., Wang, G., Banie, L., Ning, H., Shindel, A.W., Fandel, T.M., Lue, T.F., Lin, C.S., 2010.

478   Treatment of stress urinary incontinence with adipose tissue-derived stem cells. Cytotherapy. 12, 88-95.

479   Logemann, J.A., Smith, C.H., Pauloski, B.R., Rademaker, A.W., Lazarus, C.L., Colangelo, L.A.,

480   Mittal, B., MacCracken, E., Gaziano, J., Stachowiak, L., Newman, L.A., 2001. Effects of

481   xerostomia on perception and performance of swallow function. Head & neck. 23(4), 317-321.

482   Mishima, K., Inoue, H., Nishiyama,T., Mabuchi, Y., Amano, Y., Ide, F., Matsui, M., Yamada, H.,

483   Yamamoto, G., Tanaka, J., Yasuhara, R., Sakurai, T., Lee, M.C., Chiba ,K., Sumimoto, H., Kawakami,

484   Y., Matsuzaki, Y., Tsubota, K., Saito, I., 2012. Transplantation of Side Population Cells Restores the

485   Function of Damaged Exocrine Glands Through Clusterin. Stem cells. 30, 1925–1937.

486   Mohamed, D.A., Elnegris, H.M., Wahdan, R.A., 2015. Histological effect of ovariectomy and estrogen

487   replacement on parotid gland of adult albino rat. J. Histol. Histopathol. 2, 23.

488   Messina, G., Viggiano, A., De Luca, V., Messina, A., Chieffi, S., Monda, M., 2013. Hormonal Changes

489   in Menopause and Orexin-A Action. Obstet. Gynecol. Int. 209812.

490   Mortazavi, H., Baharvand, M., Movahhedian, A., Mohammadi, M., Khodadoustan, A., 2014.

491   Xerostomia due to systemic disease: a review of 20 conditions and mechanisms. Ann. Med. Health Sci.

492   Res. 4(4), 503–510.

493   Myers, R.K., McGavin, M.D., 2007. Cellular and tissue responses to injury. In McGavin M.D., Zachary,

494   J.F., Pathologic basis of veterinary disease, Fourth Edition. Mosby, St Louis, MO. pp. 3-62.

495   Parlak, S.N., Tatar, A., Keles, O.N., Selli, J., Can, I., Unal, B., 2014. Effects of menopause and diabetes

496   on the rat parotid glands: A histopathological and stereological study. Int. J. Med. Sci. Public Health.

497   3(6), 749-755.

498   Ray, R., Herring, C.M., Markel, T.A., Crisostomo, P.R., Wang, M., Weil, B., Lahm, T., Meldrum, D.R.,

499   2008. Deleterious effects of endogenous and exogenous testosterone on mesenchymal stem cell VEGF

500   production. Am. J. Physiol. Regul. Integr. Comp. Physiol. 294, R1498–R1503.

501   Rahnama, M., Swiatkowski, W., Lancut, M., Wojcik, A., 2004. Influence of raloxifene and 17

502   β-oestradiol on rats' oral mucosal structure. Bull. Vet. Inst. Pulawy. 48, 329-332.

503   Safayi, S., Korn, N., Bertram, A., Akers, R.M., Capuco, A.V., Pratt, S.L., Ellis, S., 2012. Myoepithelial

504   cell differentiation markers in prepubertal bovine mammary gland: Effect of ovariectomy. J. Dairy. Sci.

505   95(6), 2965–2976.

506   Sidney, L.E., Branch, M.J., Dunphy, S.E., Dua, H.S., Hopkinson, A., 2014. Concise Review: Evidence

507   for CD34 as a Common Marker for Diverse Progenitors. Stem cells. 32, 1380–1389.

508   Smith, J., Lindsay, M., Rahimian, R., Anderson, L., 2009. The influence of estrogen and

509   progesterone on parasympathetic vasodilatation in the rat submandibular gland. Auton. Neurosci.

510   146, 87–94.

511   Soria, B., Skoudy, A., Martín, F., 2001. From stem cells to beta cells: new strategies in cell therapy of

512   diabetes mellitus. Diabetologia. 44(4), 407–415.

513   Takahashi, M., Li, T.S., Suzuki, R., Kobayashi, T., Ito, H., Ikeda, Y., 2006. Matsuzaki M, Hamano K.

514   Cytokines produced by bone marrow cells can contribute to functional improvement of the infarcted

515   heart by protecting cardiomyocytes from ischemic injury. Am. J. Physiol. Heart. Circ. Physiol. 291(2),

516   H886–H893.

517   Takahashi, S., Nakamura, S., Shinzato, K., Domon, T., Yamamoto, T., Wakita, M., 2001.

518   Apoptosis and proliferation of myoepithelial cells in atrophic rat submandibular glands. J.

519   Histochem. Cytochem. 49(12), 1557–1563.

520   Teos, L.Y., Zheng, C.Y., Liu, X., Swaim, W.D., Goldsmith, C.M., Cotrim, A.P., Baum, B.J., Ambudkar,

521   I.S., 2016. Adenovirus-mediated hAQP1 expression in irradiated mouse salivary glands causes recovery

522   of saliva secretion by enhancing acinar cell volume decrease. Gene Ther. 23, 572-579.

523   Valimaa, H., Savolainen, S., Soukka, T., Silvoniemi, P., Makela, S., Kujari, H., Gustafsson, J.A., Laine,

524   M., 2004. Estrogen receptor-beta is the predominant estrogen receptor subtype in human oral epithelium

525   and salivary glands. J. Endocrinol. 180, 55-62.

526 Valle-Prieto, A., Conget, P.A., 2010. Human mesenchymal stem cells efficiently manage oxidative stress.

527 Stem cells Dev. 19(12), 1885-1893.

528 Walker, M.L., Herndon, J.G., 2008. Menopause in Nonhuman Primates?. Biol. Reprod. 79(3), 398–396.

529 Wan, C., He,Q., Li, G., 2006. Allogenic peripheral blood-derived mesenchymal stem cells (MSCs)

530 enhance bone regeneration in rabbit ulna critical-sized bone defect model. J. Orthop. Res. 24(4),

531 610-618.

532 Wang, Y., Schulte, B.A., LaRue, A.C., Ogawa, M., Zhou, D., 2006. Total body irradiation selectively

533 induces murine hematopoietic stem cell senescence. Blood. 107(1), 358–366.

534 Xu, L.W., Jia, M., Salchow, R., Kentsch, M., Cui, X.J., Deng, H.Y., Sun, Z.J., Kluwe, L., 2012. Efficacy

535 and Side Effects of Chinese Herbal Medicine for Menopausal Symptoms: A Critical Review. 2012, 1-19.

536 Yeh, C.K., Johnson, D.A., Dodds, M.W.J., 1998. Impact of aging on human salivary gland

537 function: a community-based study. Aging Clin Exp Res. 10(5), 421-428.

538 Zhang, D., Yang, B., Zou, W., Lu, X., Xiong, M., Wu, L., Wang, J., Gao, J., Xu, S., Zou, T., 2012.

539 Estradiol synthesis and release in cultured female rat bone marrow stem cells. BioMed. Res. Int. 2013,

540 301540.

541 Zhao, Q., Ren, H., Han, Z., 2016. Mesenchymal stem cells: Immunomodulatory capability and

542 clinical potential in immune diseases. JOCIT. 2(1), 3-20.

543 Zheng, W., Liu, D., Fan, X., Powers, L., Goswami, M., Hu, Y., Lin, P., Medeiros, L. J., Wang, S. A.,

544 2013. Potential Therapeutic Biomarkers in Plasma Cell Myeloma: A Flow Cytometry Study. Cytometry

545 Part B. 84B, 222–228.

546

547

548

549

550

551

552

553

554 **Figure Legends**

555 **Fig. 1** Identification of the hUCB-MSCs. A photomicrograp of the culture at day 7 of isolation

556 showing a fusiform-shaped morphology of cells (solid arrows) (A). Histograms of flow cytometric

557 analysis of the hUCB-MSCs culture, showing positive expressions for human CD105 (85.65%) and

558 human CD90 (62.33%) depending on 20% cutoff, while negative expressions for human CD34

559 (1.36%) and human CD45 (2.19%). Open histogram indicates the negative control background

560 signal; positive reactivity is displayed in shaded histogram (B).

561 **Fig. 2** Immunofluorescence analysis. Immunofluorescence detection of the homing of the

562 PKH26-labelled hUCB-MSCs around the acini (solid arrows) and ducts (dashed arrows) in the

563 parotid glandular tissues of the OVX + hUCB-MSCs group (3 months post-ovariectomy) is noticed

564 (A, B). Immunohistochemical detection of the hUCB-MSCs homing in sections of parotid glands

565 express a positive reaction with anti-human CD 105 around acini (solid arrows) and duct (dashed

566 arrows) (C) but a negative reaction with anti-human CD 34 (D).

567 **Fig. 3** Histomorphological features of the parotid glands. Representative histopathological

568 photomicrographs of H&E stained parotid glandular tissues of the SHAM group (A), OVX group

569 (B), and OVX + hUCB-MSCs group (C) showing serous acini (S), intercalated ducts (white

570 arrowheads), striated duct (SD) with a prominent basal striation (solid arrows), intracytoplasmic

571 vacuoles (black arrowheads), crescent-shaped nucleus (dashed arrow), and interstitial space with

572 hemorrhage (Hg).

573 **Fig. 4** Proliferating cell populations in the parotid glands. Immunohistochemical photomicrographs showing

574 PCNA positive cells (arrows) in the acini of SHAM group (A), OVX group (B), and OVX + hUCB-MSCs

575 group (C). The negative control stained section of the SHAM group in which the primary antibody is

576 replaced by PBS (D). Bar chart showing the average number of PCNA positive cells of different groups (E).

577 Each bar carrying different superscripts letters (a, b, and c) are significantly different as analyzed by the

578 one-way ANOVA test, followed by the multiple comparisons Duncan's Post-hoc test ($P < 0.05$); n = 6 in

579 each experimental group. Values = mean ± SE.

580 **Fig. 5** Apoptotic cell populations in the parotid glands. Immunohistochemical photomicrographs showing

581 Caspase 3 positive cells (arrows) in the interstitial tissues of SHAM group (A), OVX group (B) and OVX +

582 hUCB-MSCs group (C). The negative control stained section of the OVX group in which the primary

583   antibody is replaced by PBS (D). Bar charts showing the average number of Caspase 3 positive (E) and

584   ssDNA positive apoptotic cells in different groups (F). Each bar carrying different superscripts letters (a, b

585   and c) are significantly different as analyzed by the one-way ANOVA test, followed by the multiple

586   comparisons Duncan's Post-hoc test (P < 0.05); n = 6 in each experimental group. Values = mean ± SE.

587   **Fig. 6** Blood capillary populations in the parotid glands. Immunohistochemical photomicrographs showing

588   AQP1 positive blood capillaries in between the acini (arrows) and around striated ducts (arrowheads) of the

589   SHAM group (A), OVX group (B), and OVX + hUCB-MSCs group (C). The negative control stained

590   section of the SHAM group in which the primary antibody is replaced by PBS (D). Bar chart showing the

591   integrated density ratio of AQP1 positive blood capillaries in different groups (E). Each bar carrying different

592   superscripts letters (a, b and c) are significantly different as analyzed by the one-way ANOVA test, followed

593   by the multiple comparisons Duncan's Post-hoc test (P < 0.05); n = 6 in each experimental group. Values =

594   mean ± SE.

595   **Fig. 7** Myoepithelial cell populations in the parotid glands. Immunohistochemical photomicrographs

596   showing α-SMA positive cells with their cytoplasmic processes around the acini (arrows) and intercalated

597   duct (arrowhead) of SHAM group (A), OVX group (B), and OVX + hUCB-MSCs group (C). The negative

598   control stained section of the SHAM group in which the primary antibody is replaced by PBS (D). Bar chart

599   showing the integrated density ratio of distribution of α-SMA positive cells in different groups (E). Each bar

600   carrying different superscripts letters (a, b and c) are significantly different as analyzed by the one-way

601 ANOVA test, followed by the multiple comparisons Duncan's Post-hoc test (P < 0.05); n = 6 in each

602 experimental group. Values = mean ± SE.

603 **Fig. 8** Endogenous hematopoietic progenitor cell populations in the parotid glands. Immunohistochemical

604 photomicrographs showing anti-mouse CD34 positive cells surrounding acini (arrows) and striated ducts

605 (arrowheads) of SHAM group (A), OVX group (B), and OVX + hUCB-MSCs group (C). Insets indicate

606 immunopositive reaction of hematopoietic progenitor cells that have large nucleus with little cytoplasm. The

607 negative control stained section of the SHAM group in which the primary antibody is replaced by PBS (D).

608 Bar chart showing the average number of mouse CD34 positive cells in different groups (E). Each bar

609 carrying different superscripts letters (a, b and c) are significantly different as analyzed by the one-way

610 ANOVA test, followed by the multiple comparisons Duncan's Post-hoc test (P < 0.05); n = 6 in each

611 experimental group. Values = mean ± SE.
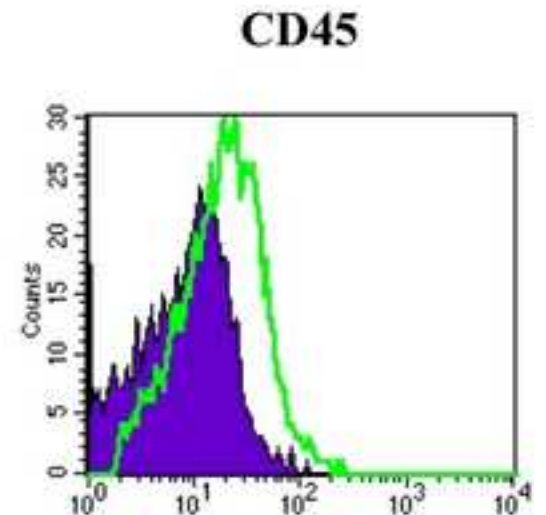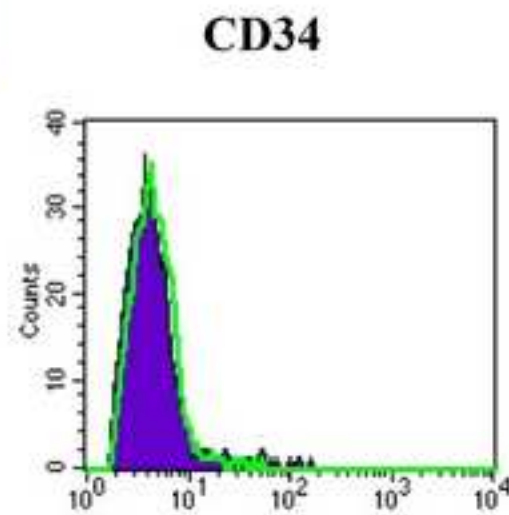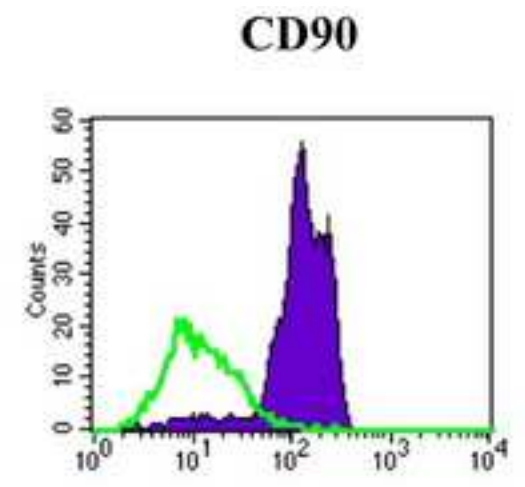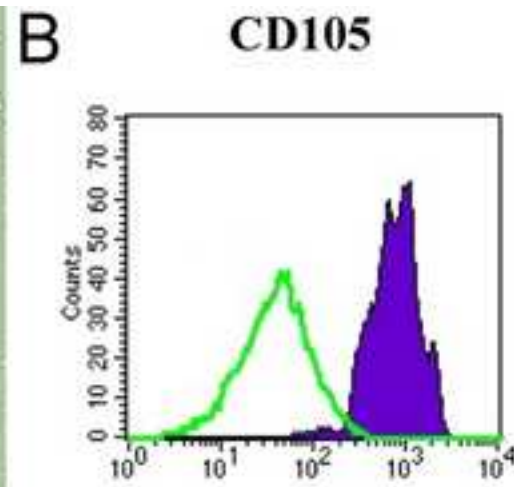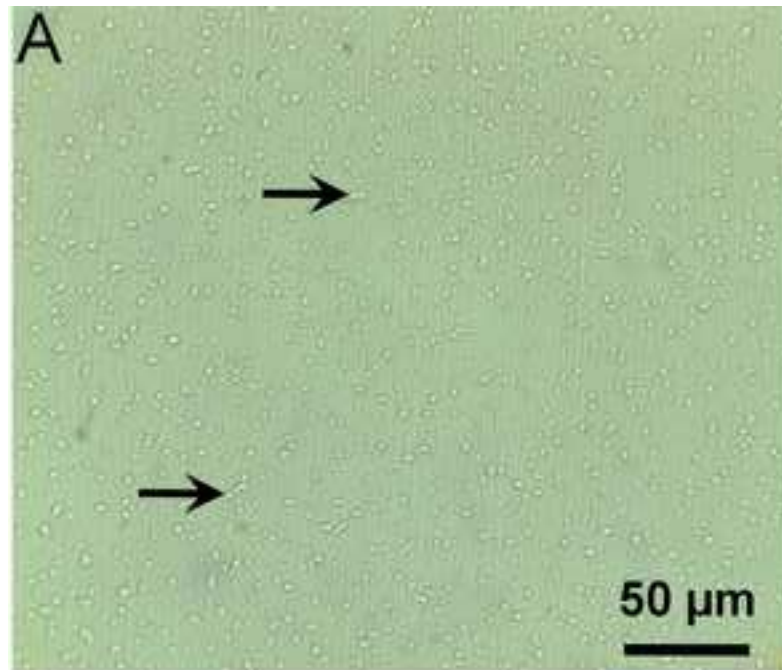
A

50 µm

B

50 µm

C

50 µm

D

50 µm

E

Caspase 3⁺ cells

Number

14
12
10
8
6
4
2
0

a

b

c

SHAM   OVX   OVX+hUCB-MSCs

F

ssDNA⁺ cells

Number

140
120
100
80
60
40
20
0

a

b

b

SHAM   OVX   OVX+hUCB-MSCs

A

50 µm

D

50 µm

B

50 µm

C

50 µm

E   X 10⁶   AQP1⁺ cells

SHAM   OVX   OVX+hUCB-MSCs
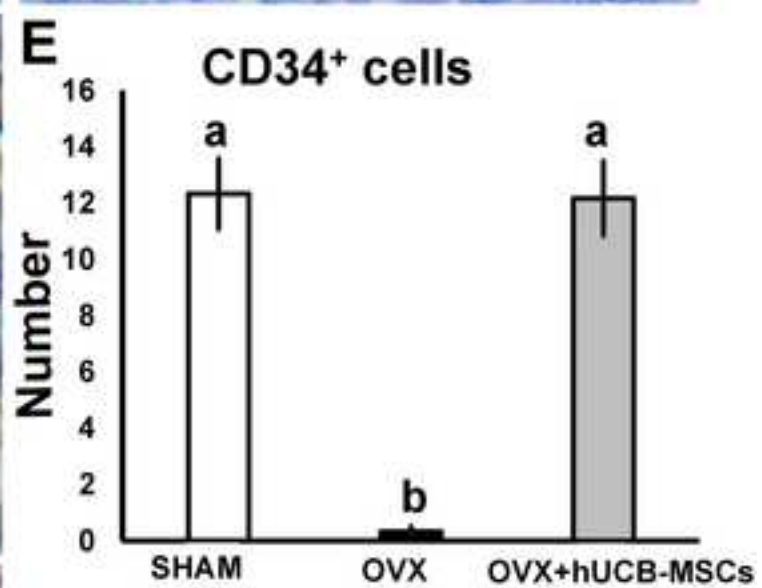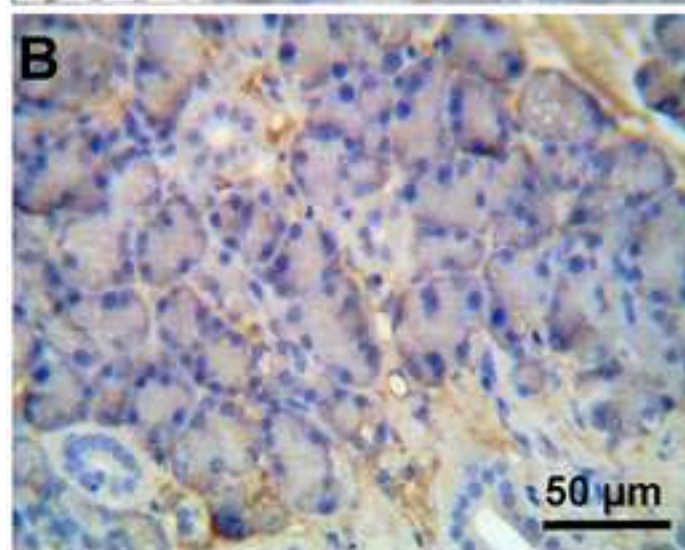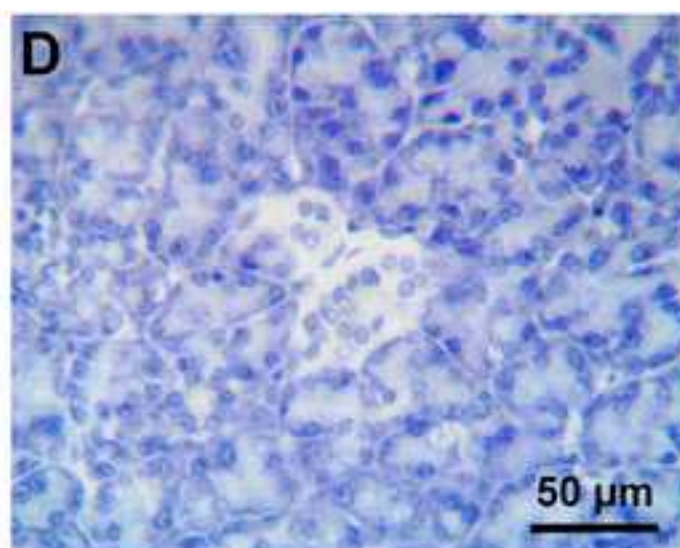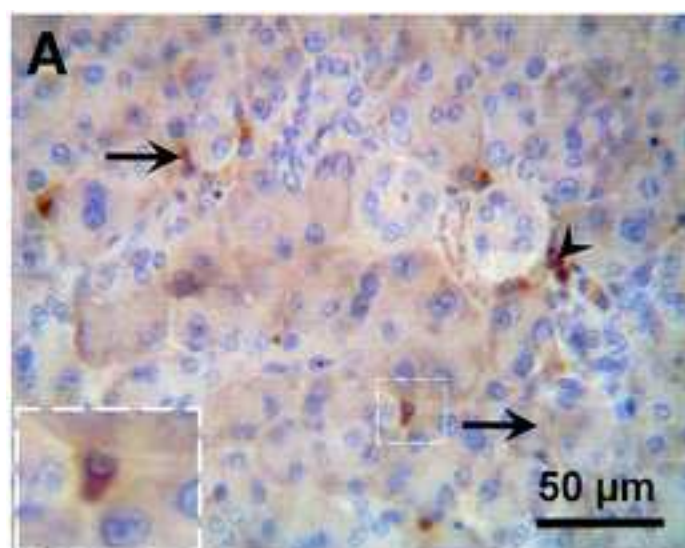
E

Myoepithelial⁺ cells
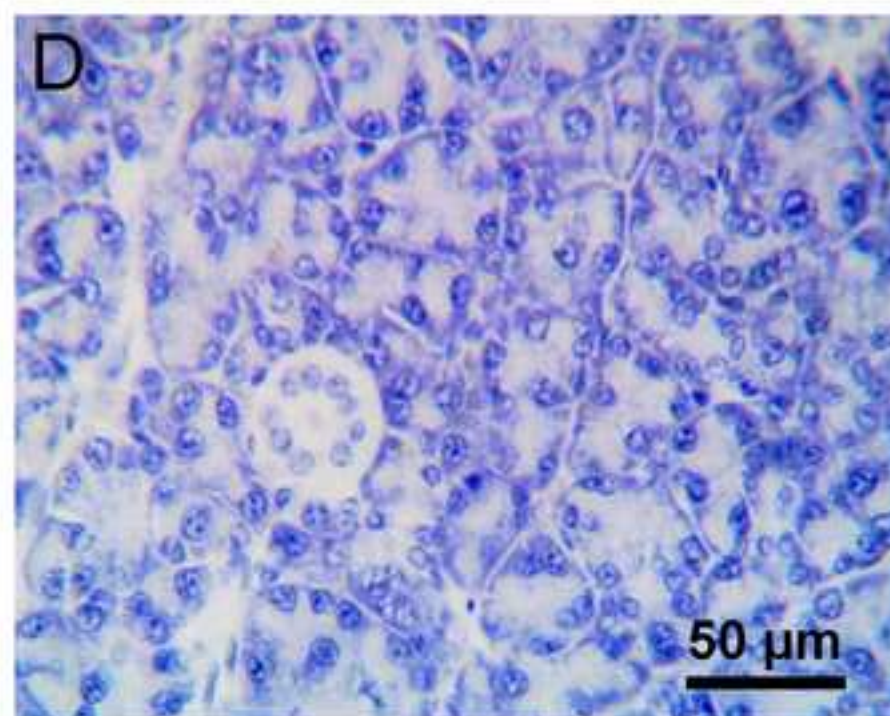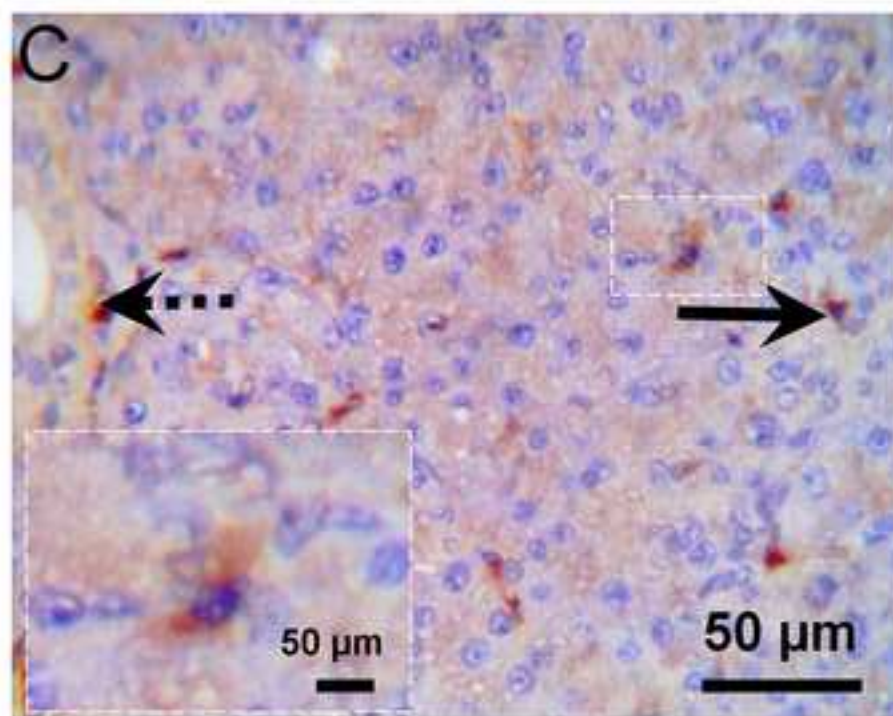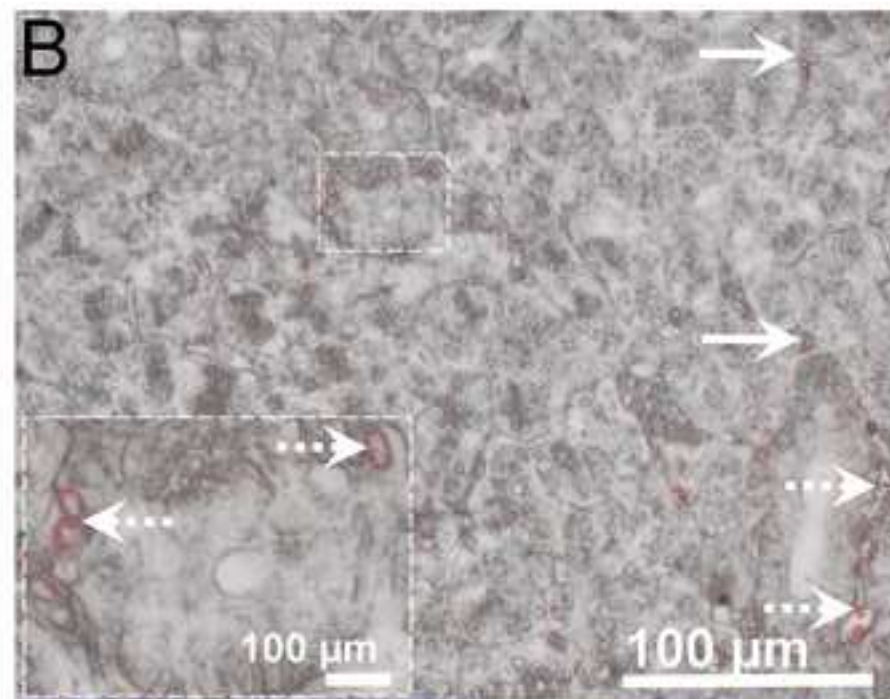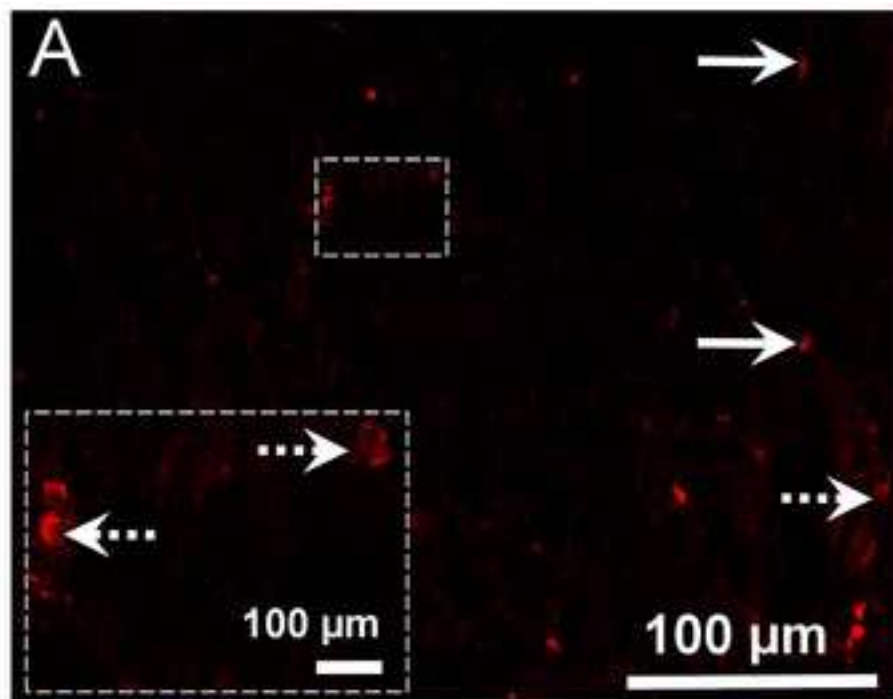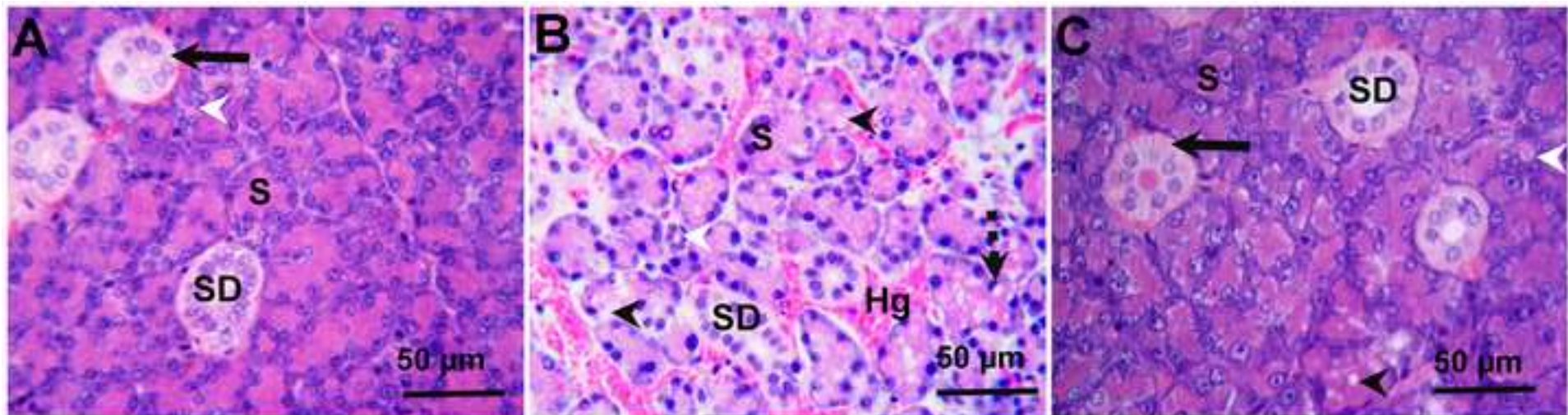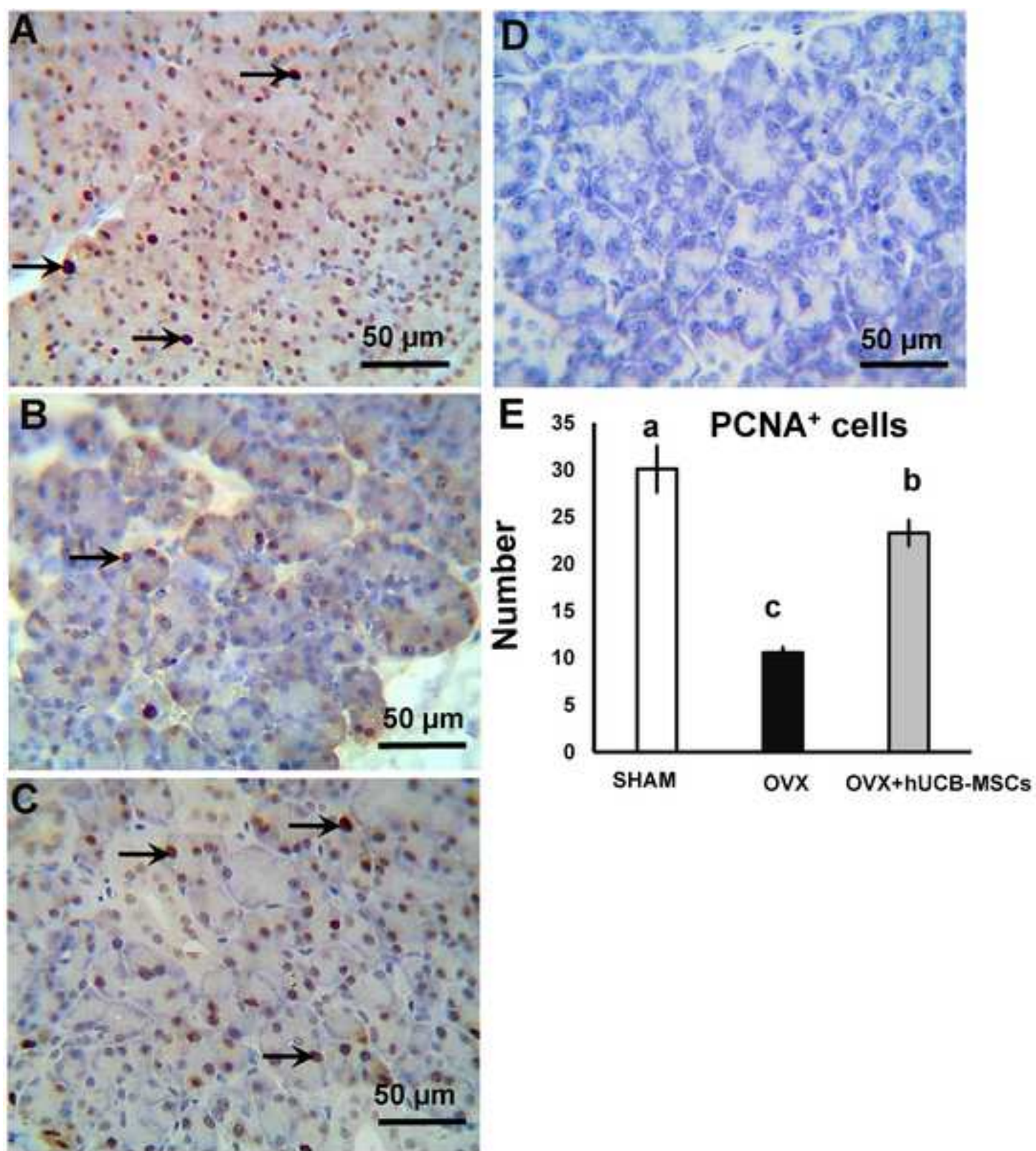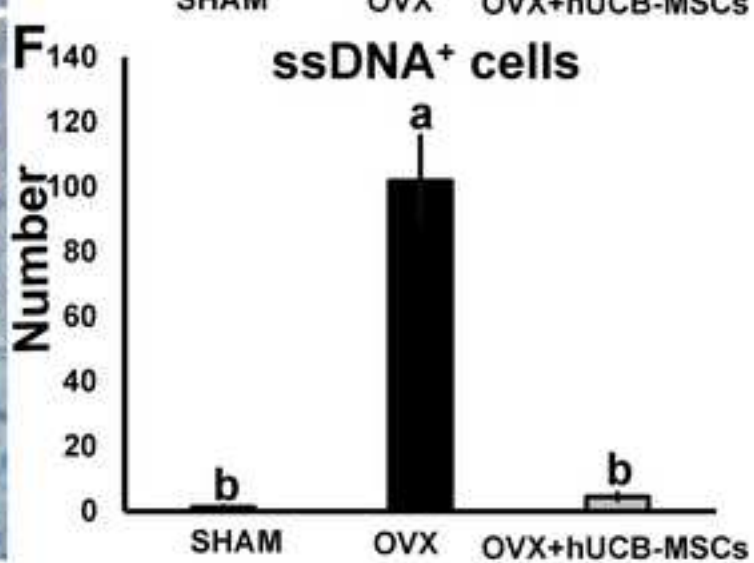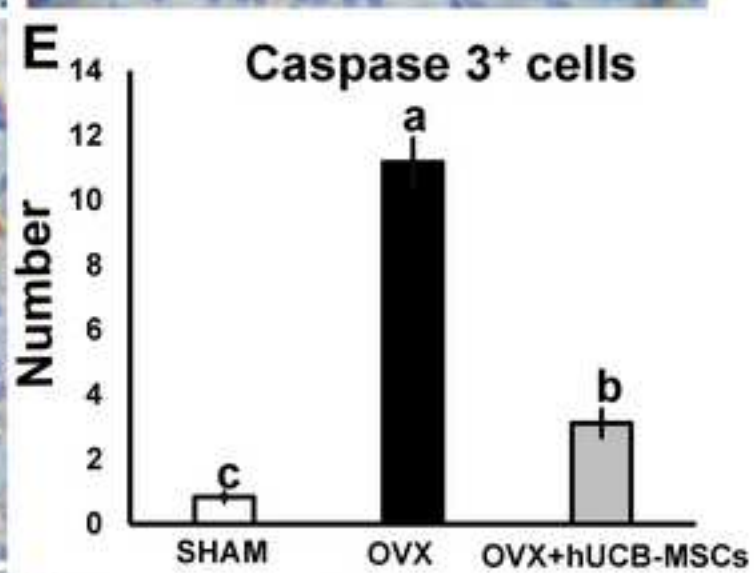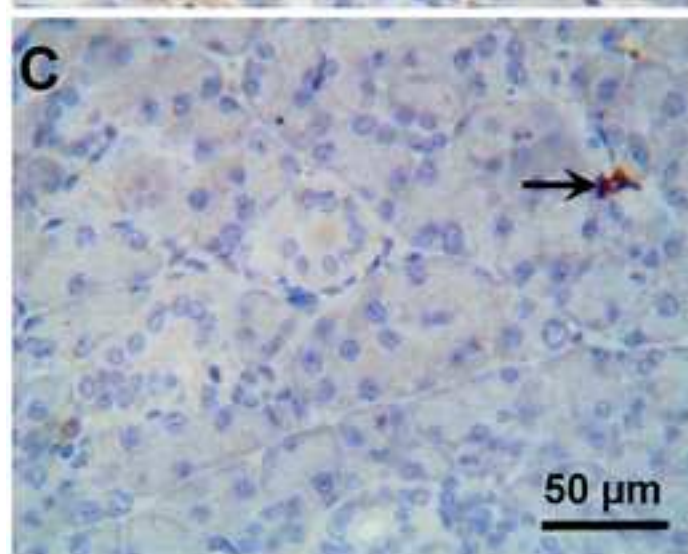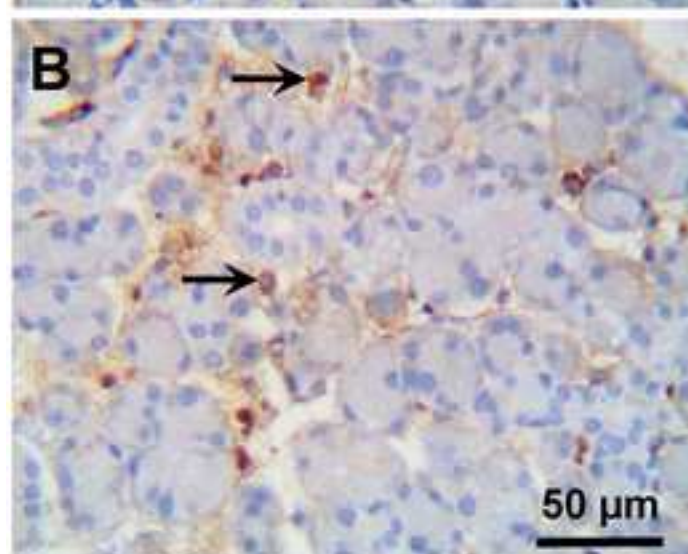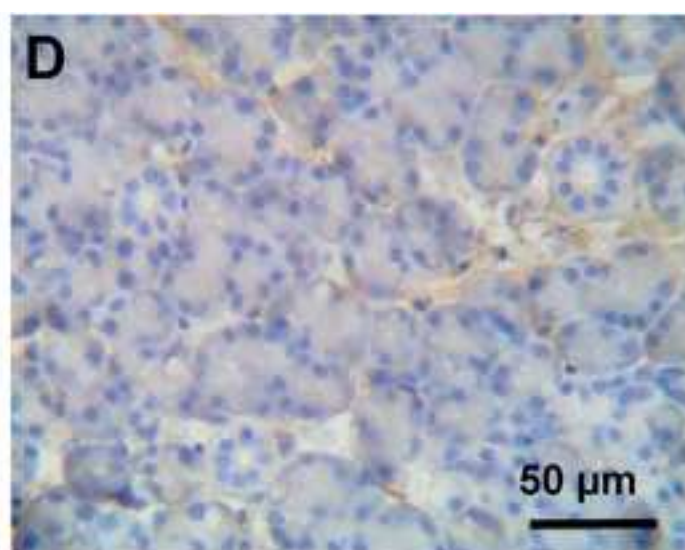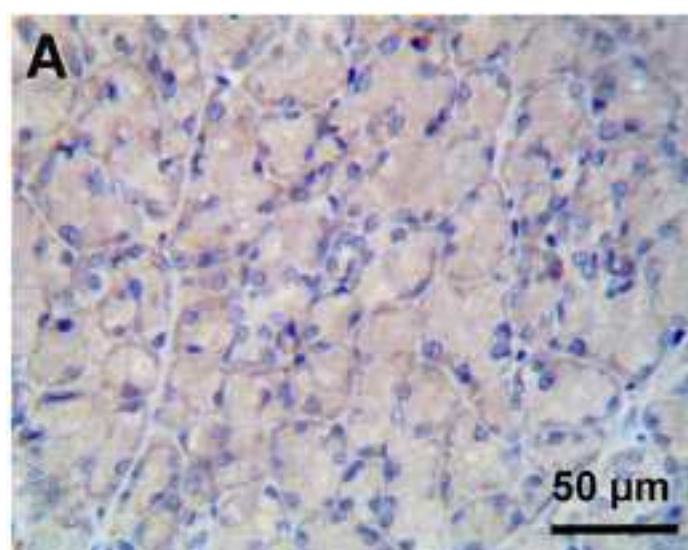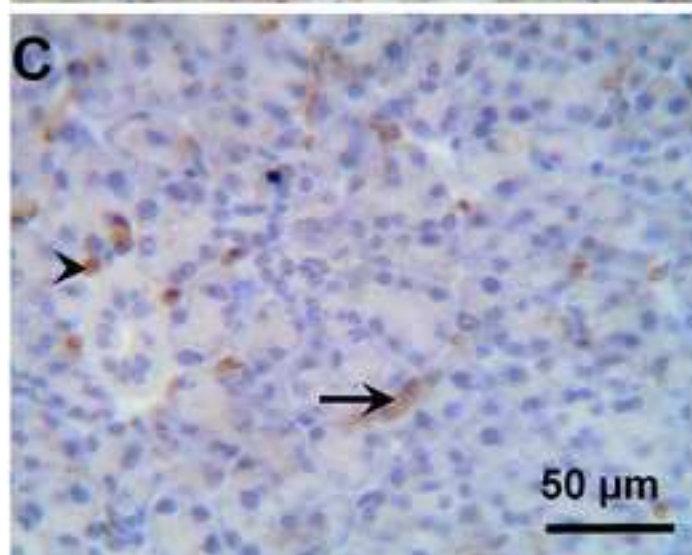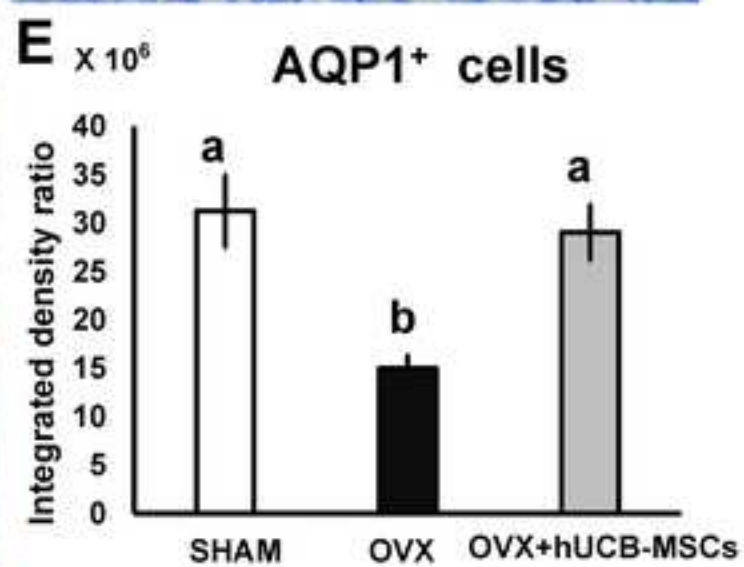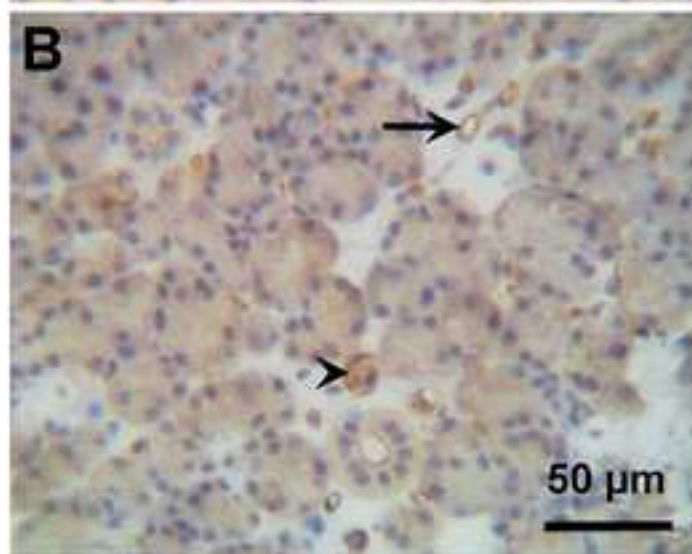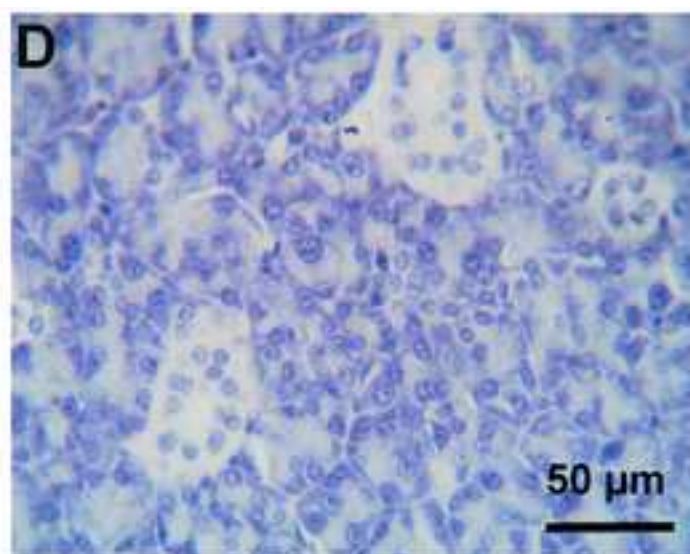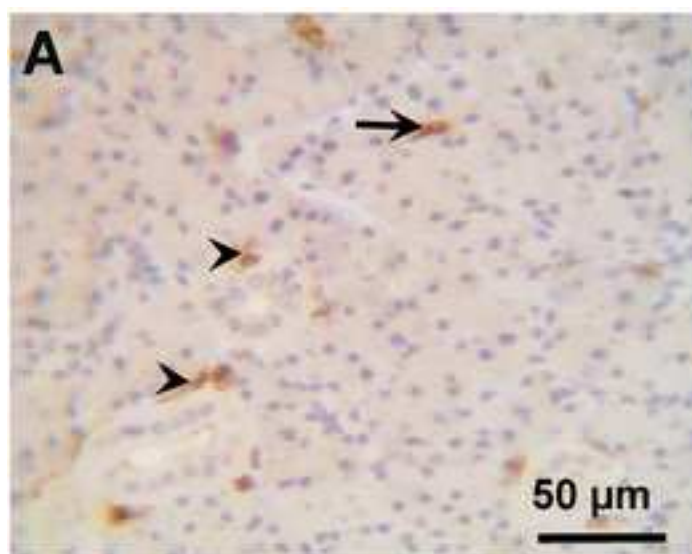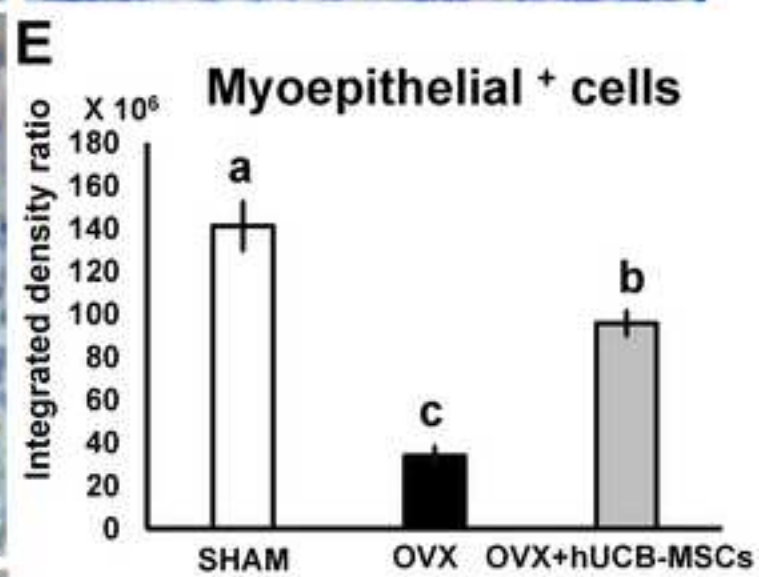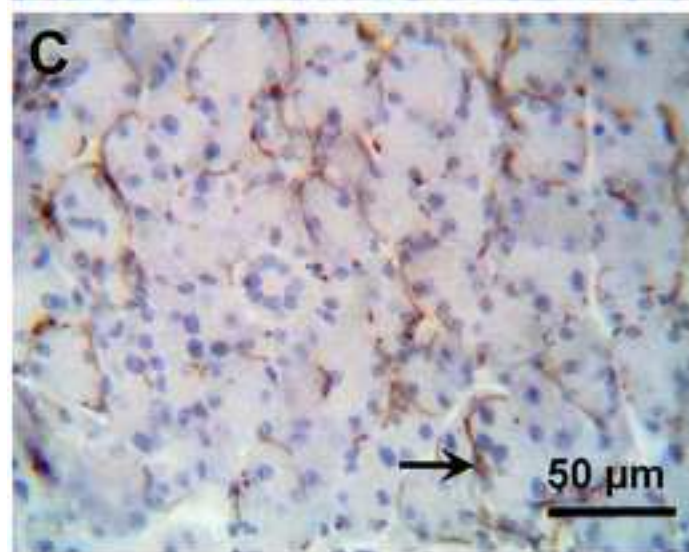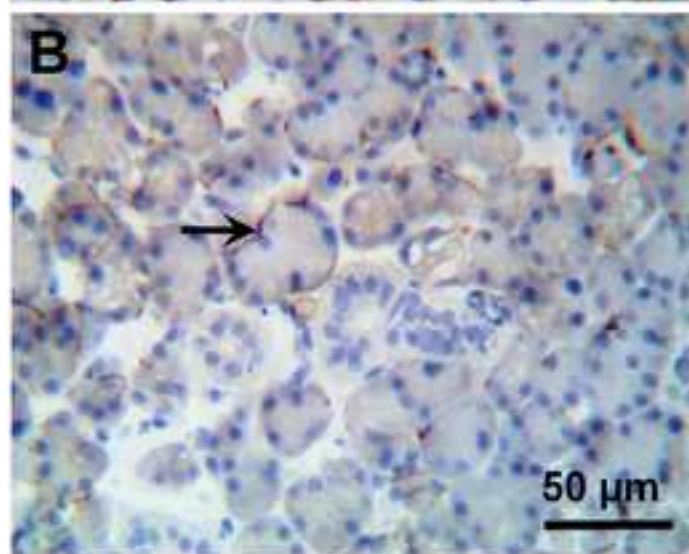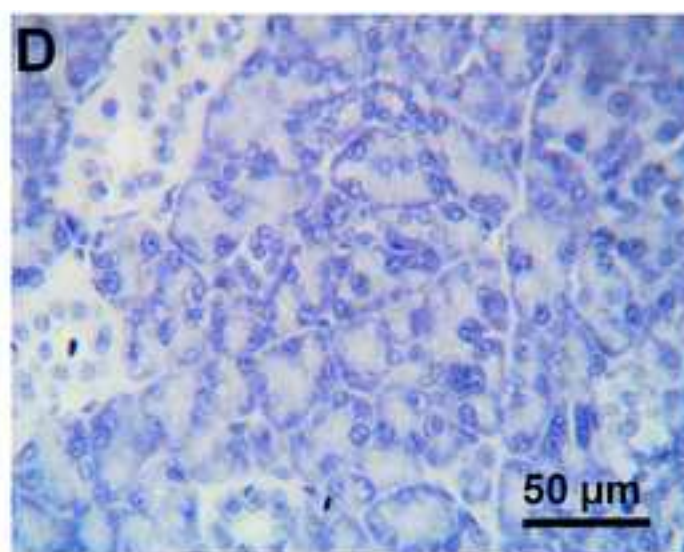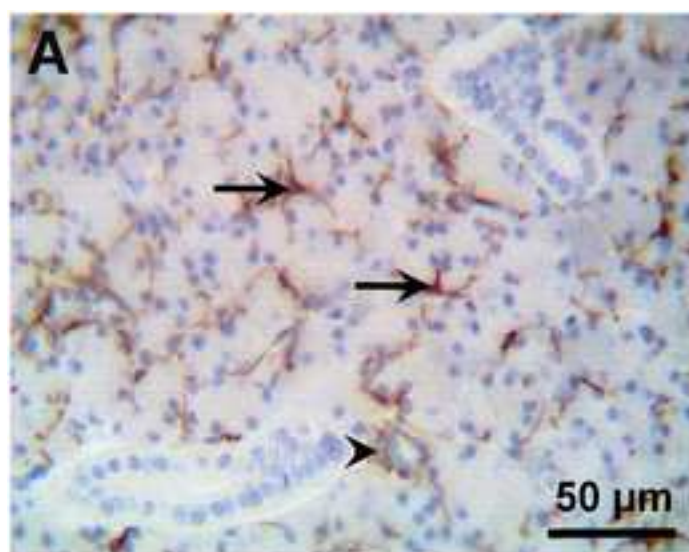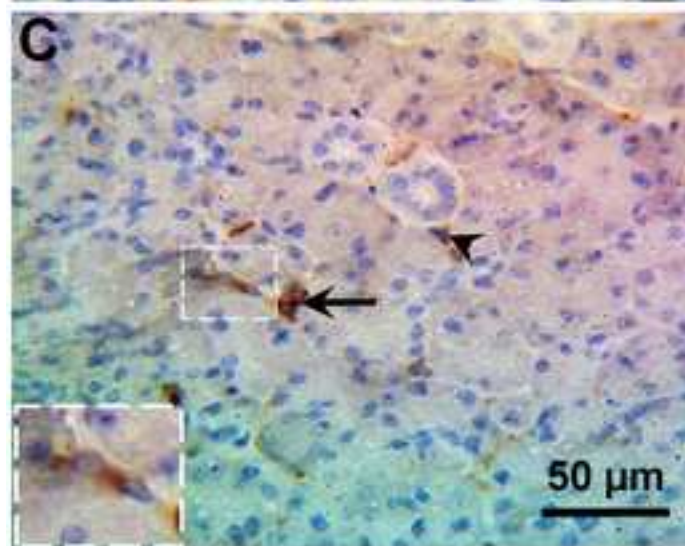
Table

Table 1 A list of antibodies, sources, working dilutions, and antigen retrieval.

Antibodies	Sources	Dilutions	Antigen retrieval, temperature, time
Anti-human CD105: SN6h	Gennova Scientific SLc	1:200	Citrate buffer (pH 6.0),95℃, 20 min.
Anti-humanCD34: QBEnd/10	Gennova Scientific SLc	1:400	Citrate buffer (pH 6.0),105℃, 20 min.
Monoclonal anti-goat PCNA	Santa Cruz Biochemistry, (Santa Cruz, USA)	1:2000	Dako, 105℃, 20 min.
Anti-rabbit ssDNA	IBL – Fujioka, japan	1:200	No antigen retrieval used, don't Autoclave.
Anti-rabbit AQP1	Santa Cruz	1:50	2XSSC, 105℃, 20 min.
Anti-rabbit α-SMA	Abcam, Cambridge, UK	1:3000	Citrate buffer (pH 6.0),105℃, 20min.
Anti-rabbit Caspase 3	IMGENEX	1:800	2XSSC, 105℃, 20min.
Anti-mouse CD34	Abcam	1:400	Citrate buffer,105℃ 20min.

Table 2 Statistical analysis of salivary flow rate and weight of parotid glands in all investigated groups.

Parameters	SHAM	OVX	OVX+hUCB-MSCs
Salivary flow rate (μl/min)	$48.08{\pm}3.07^{a}$	$10.03{\pm}1.10^{b}$	$43.85{\pm}3.56^{a}$
parotid glands' weight (mg)	$303.65{\pm}12.72^{a}$	$175.43{\pm}6.49^{b}$	$280.58{\pm}8.82^{a}$

Data are expressed as the mean ± SD.
Different superscripts indicate significant difference at $p < 0.05$ by one-way ANOVA followed by the multiple comparisons Duncan's Post-hoc test for analysis of difference among different groups.